# Bistatic noise radar: Demonstration of correlation noise suppression



Citation for the original published paper (version of record):

Ankel, M., Jonsson, R., Bryllert, T. et al (2023). Bistatic noise radar: Demonstration of correlation noise suppression. IET Radar, Sonar and Navigation, 17(3): 351-361.
http://dx.doi.org/10.1049/rsn2.12345



(article starts on next page)

Received: 21 July 2022 | Revised: 14 October 2022 | Accepted: 16 October 2022

DOI: 10.1049/rsn2.12345

IET Radar, Sonar & Navigation

The Institution of Engineering and Technology WILEY

ORIGINAL RESEARCH

# Bistatic noise radar: Demonstration of correlation noise suppression

Martin Ankel[1,2] | Robert Jonsson[1,2] | Tomas Bryllert[1,2] | Lars M. H. Ulander[3] | Per Delsing[1]

[1]Department of Microtechnology and Nanoscience, Chalmers University of Technology, Göteborg, Sweden

[2]New Concepts and System Studies, Surveillance, Saab, Göteborg, Sweden

[3]Department of Space, Earth and Environment, Geoscience and Remote Sensing, Chalmers University of Technology, Göteborg, Sweden

**Correspondence**

Martin Ankel, Department of Microtechnology and Nanoscience, Chalmers University of Technology, Göteborg, 41296 Sweden.
Email: ankel@chalmers.se

**Funding information**

Saab, Grant/Award Number: N/A; Knut och Alice Wallenbergs Stiftelse, Grant/Award Number: KAW 1017.0449

**Abstract**

In this study, spatial separation of the radar transmitter and receiver units is considered, as a means of reducing the masking effect in noise radars. A bistatic radar system is constructed, with emphasis on a lightweight transmitter unit that can be mounted on a commercial Unmanned Aerial Vehicle (UAV). The system uses pseudo-random noise, generated digitally at the receiver and transmitter units. Correlation losses, due to non-linearities in the transmitter and receiver units, are measured to 0.1 dB. This study shows that by separating the transmitter and receiver unit the masking effect is significantly reduced, compared to a monostatic setup. This reduction is enough for the system to detect a slow flying UAV. Thus, bistatic separation should be considered as a practical tool to reduce the masking effect. By processing clutter with an extended CLEAN algorithm, the correlation noise floor is further suppressed.

## 1 | INTRODUCTION

The utilisation of non-periodic random waveforms for radar has several benefits, such as favourable ambiguity function [1–3], low probability of intercept/identification (LPI/LPID) [4–6], and low mutual interference [5, 7]. The idea of transmitting noise waveforms and estimating the range by correlation processing was proposed already back in 1959 [8].

Despite the benefits offered by noise radars, the fact that the field has been around for more than 6 decades and multiple proof-of-concept experiments have been performed [9–17], to our knowledge, a full commercial or military system has yet to be realised. The reason is probably that noise radar also comes with several challenges or drawbacks. One such drawback is that the correlation integral produces a substantial noise floor [18–20] limiting the system's detection sensitivity, often referred to as the masking effect. For clarity, we refer to the masking effect as the *correlation noise floor* (CNF). The CNF, relative to the strongest scatterer, is closely related to the time-bandwidth product of the waveform. This means that, for a small time-bandwidth product, a strong signal return will mask weaker returns. This is particularly detrimental when interference due to strong clutter is present. For a monostatic ground-based continuous wave radar system, this is almost always the case.

There are several different techniques to alleviate the CNF problem, all coming with their own drawbacks. There are algorithms such as lattice filters [21, 22], estimating and subtracting clutter echoes [23–28], CLEAN [29, 30], mismatched filtering [25, 31], inverse filtering [32, 33], Wiener filtering [34] and apodisation filtering [35]. Most of these techniques require immense processing power, which makes them difficult to implement in real time. Furthermore, the system and operation can be adjusted, for example, waveform design [36–40], pulsed operation, shielding between antennas, and increasing the time-bandwidth product. Another solution is to spatially separate the receiver and transmitter units, that is, bistatic noise radar. The separation of receiver and transmitter units, depending on the geometry, will lead to a significant reduction in close range clutter interference, without requiring additional processing power. Additionally, all the clutter reduction and pulse shaping techniques mentioned above can still be applied to reduce residual interference.

Bistatic radar has in the past proven to be a difficult endeavour, for numerous reasons [41–43]. However, thanks to the development of multi-channel digital radars, bistatic operation is significantly simplified. Digital radars can also operate with arbitrary waveforms, including noise waveforms. A monostatic pulse Doppler radar can, therefore, operate as receiver in combination with a bistatic noise transmitter. Noise radar operation would then be a complement to traditional pulsed operation, and not an independent system. The flexibility in choosing between LPI properties and detection performance could be the necessary component for noise radars to become commercially viable, especially as the transmitter can be made cheap. However, bistatic operation, in general, comes with its own difficulties. In particular, there are challenges in achieving time and frequency synchronisation.

Previous work [44, 45] has realised proof-of-principle bistatic noise radar systems. These experiments demonstrated the bistatic setup for relatively small separations, showing frequency synchronisation between transmitter and receiver could be maintained with global navigation satellite system (GNSS). In these experiments, pseudo-random noise is used as the noise source. This makes it possible to digitally generate the reference at the receiver unit, thus simplifying the system design by avoiding a reference antenna and eliminating the risk of disturbances contaminating the reference channel [46]. It does, however, impose requirements on the linearity of the system as non-linear behaviour will distort the signal leading to a loss through the reference mismatch.

In this work, we have constructed a flexible bistatic noise radar transmitter. With this system, we show the reduction in close range clutter, by comparing the bistatic setup with a monostatic reference system, in a difficult clutter environment. As a post-processing step, we have implemented a version of the CLEAN algorithm for clutter suppression, achieving a lower CNF by up to 20 dB.

The article is organised as follows. Section 2 summarises the theory for the bistatic setup and the signal model to explain the clutter suppression algorithm. Section 3 presents the bistatic demonstrator hardware and signal processing. The scenario and experimental results are presented in Section 4 and Section 5 respectively. Finally, we conclude with a discussion on the aspects of applications and outlook in Section 6.

## 2 | THEORY

### 2.1 | Radar fundamentals

To introduce the relevant quantities and to give context to the experiment, we present some theory of bistatic noise radar. The bistatic noise radar range equation is given by [22]

$$R_R R_T = \sqrt{\frac{P_T G_T G_R \lambda^2 \tau_I \sigma}{(4\pi)^3 L k_B T_0 F (\mathrm{SNR})_0}}, \tag{1}$$

where $R_T$ is the transmitter to target distance, $R_R$ is the receiver to target distance, $P_T$ is the transmitted power, $G_T$ is the transmitter antenna gain, $G_R$ is the receiver antenna gain, $\lambda$ is the wavelength, $\tau_I$ is the integration time, $\sigma$ is the target bistatic radar cross section (RCS), $L$ is the losses, $k_B$ is Boltzmann's constant, $T_0$ is the reference temperature, $F$ is the noise figure, and $(\mathrm{SNR})_0$ is the detection threshold. By setting $R_T = R_R$, we get the monostatic radar range equation.

In a bistatic configuration, the Doppler shift is given by [42]

$$f_D = 2\,\frac{v}{\lambda}\cos\left(\frac{\varphi}{2}\right)\cos(\delta), \tag{2}$$

where $v$ is the target's speed, $\varphi/2$ is the bistatic bisector and $\delta$ is the angle between the target's velocity vector and the bistatic bisector, see Figure 1. For $\varphi = 0$, the monostatic Doppler shift is obtained.

High bandwidth noise radars will suffer from degradation in Doppler resolution, according to [47]

$$\Delta v = \lambda\sqrt{(2\tau_I)^{-2} + 4(v - v_r)^2 (B/c)^2}, \tag{3}$$

where $B$ is the signal bandwidth and where $v_r$ is the velocity of the digital reference signal, that is, the velocity used by the matched filter ($v_r = 0$ in this experiment). By resampling the reference to match the Doppler shift of the moving target, that is, setting $v_r = v$, the same Doppler resolution as for a coherent Doppler radar would be obtained. Resampling of the reference for this purpose is referred to as stretch processing [48]. Noise radars also suffer from low Doppler tolerance [49], but if the correlation times are kept short enough, this issue can be neglected.

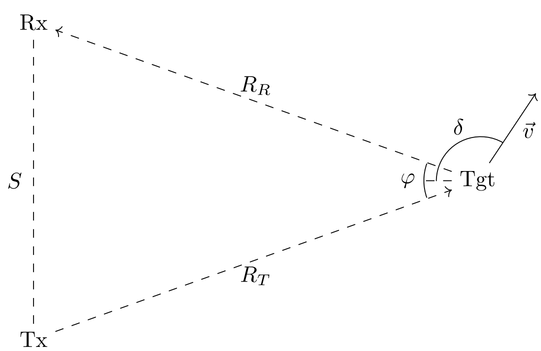


**FIGURE 1** Bistatic geometry where the transmitter (Tx) and receiver (Rx) are separated by a distance $S$. The transmit-to-receive distance to the target (Tgt) is $R_T + R_R$, where the geometry defines a bistatic separation angle $\varphi$. The target speed in the bistatic plane $v$ is defined in a direction $\delta$ relative to the bistatic bisector.

## 2.2 | Signal model

In this section, we present a model for the transmit-to-receive channel. The model assumes that clutter scatters in a range of Doppler frequencies centred around zero. We assume the transmitter continuously sends a signal $x_n$ consisting of wide-band pseudo-random noise exhibiting both amplitude and phase fluctuations. Our experimental setup uses band-limited complex Gaussian pseudo-random noise. The pseudo-random noise seed as well as the transmitter characteristics are known to the receiver, such that the transmitted signal $x_n$ can be reproduced digitally and used as reference. This removes the need to measure a reference signal from the transmit-to-receive channel.

We assume a simple model for a single non-fluctuating point target in clutter by making a narrowband approximation and neglecting range-bin migration. Explicitly, the received signal $y_n$, with one target and many clutter scatterers, is

$$y_n = \alpha x_{n-k} \mathrm{e}^{-2\pi \mathrm{i} f_{\mathrm{D}} n/f_s} + \nu_n + \sum_{\substack{i \in \{\text{range}\} \\ j \in \{\text{Doppler}\}}} \beta_{i,j} x_{n-i} \mathrm{e}^{-2\pi \mathrm{i} f_j n/f_s}, \quad (4)$$

where $\nu_n$ is the internal receiver noise, $f_s$ is the sample rate, $f_j$ is the clutter Doppler frequency, and where $\alpha, \beta_{i,j} \in \mathbb{C}$ for all $i, j, k \in \mathbb{N}$. That is, the target signal with amplitude $\alpha$ has a delay of $k$ samples with respect to the reference. The third term of Equation (4) collects clutter such that the coefficients $\beta_{i,j}$ describe the amplitude of point scatterers. We take the clutter Doppler spread to be a Gaussian shaped spectrum, that is, $\beta_{i,j} \propto \mathrm{e}^{-f_j^2/2\Delta f^2}$, with width $\Delta f$.

We emphasise some important limitations of the signal model presented in Equation (4). For one, the model holds only for the scenario when both the transmitter and receiver are stationary. If, for example, the transmitter is moving, the observed clutter will exhibit Doppler shifts, up to the speed of the transmitter, depending on the bistatic geometry. For fast moving targets, the assumption of a fixed delay $k$ fails, and range bin migration must be considered. Furthermore, the assumption of Gaussian shape clutter spectrum with fixed spectral width is not realistic for any general clutter environment, but we find it sufficient to understand this experimental scenario.

Unintended modulation of the transmitted signal (e.g., by amplifier non-linearities) will lead to a correlation loss ($L_{\mathrm{corr}}$) because of the induced mismatch between the reference $x_n$ and actual signal $\tilde{x}_n$. We take $L_{\mathrm{corr}}$ to be the loss in Peak-to-Average Ratio (PAR) of the crosscorrelation function $r_{x\tilde{x}}$ compared to the autocorrelation function $r_{xx}$. That is, the correlation loss is defined as

$$L_{\mathrm{corr}} = \frac{\mathrm{PAR}\left(r_{x\tilde{x}}\right)}{\mathrm{PAR}(r_{xx})}, \quad (5)$$

where $\mathrm{PAR}(r) = 2\tau_I \max(|r(t)|) / \int_{-\tau_I}^{\tau_I} \mathrm{d}t |r(t)|$. A low correlation loss indicates that the local receiver reference signal matches what is transmitted. This measure is suitable to characterise the receiver's and the transmitter's analog signal chain.

## 2.3 | Clutter suppression

In the setting we consider here, there is significant interference from clutter close to the receiver, in both the monostatic and bistatic setup. This interference can be several orders of magnitude stronger than the signals reflected from any targets of interest. Because of the CNF, local clutter reduces global detection performance, even after Doppler processing. A notch filter (e.g., moving target indicator), as applied in many radar systems, is insufficient here, because the CNF is unaffected. Preferably, clutter suppression should also reduce the CNF. With knowledge of the scattering coefficients $\beta_{i,j}$ of Equation (4), the signal can be processed by simply subtracting the clutter. This idea is the intuition behind the CLEAN algorithm [50]. Here, we have implemented a modification of the CLEAN algorithm for clutter suppression. In particular, we run CLEAN by estimating the strongest clutter point, subtracting its contribution and then repeating the process sequentially. For each iteration, the 1-lag distance bin and a few Doppler bins are processed by an orthogonalised reference to account for multipath and phase variations. This is implemented as a two-stage adaptive filter bank [21, 22]. The algorithm, which we refer to as Sequential CLEAN, is expected to perform well in a clutter environment that is relatively sparse and point-like, such that the strongest scattering point can be estimated and subtracted independently of other clutter. To illustrate the idealised performance and to validate the implementation, we have run Sequential CLEAN on model data based on Equation (4), see Figure 2. This implementation of Sequential CLEAN is computationally expensive, and not applicable for real-time implementation.

# 3 | HARDWARE AND SIGNAL PROCESSING

In order to experimentally verify the usefulness of a bistatic noise radar system, a complete system with one spatial channel was developed. Emphasis was put on constructing a mobile, low weight, and flexible transmitter unit, whereas the receiver unit was constructed from available lab components. The system was designed to operate in the L-Band (1.3 GHz) out of convenience (available components, direct sample synthesising, electromagnetic considerations etc.) and the choice of frequency is not necessarily optimal for noise radar operation.

In this section, we will first describe the transmitter, followed by a brief description of the receiver. Then, the waveforms and sampling frequencies used are detailed. Finally, we describe the signal processing implemented. A block diagram of the complete system is presented in Figure 3.

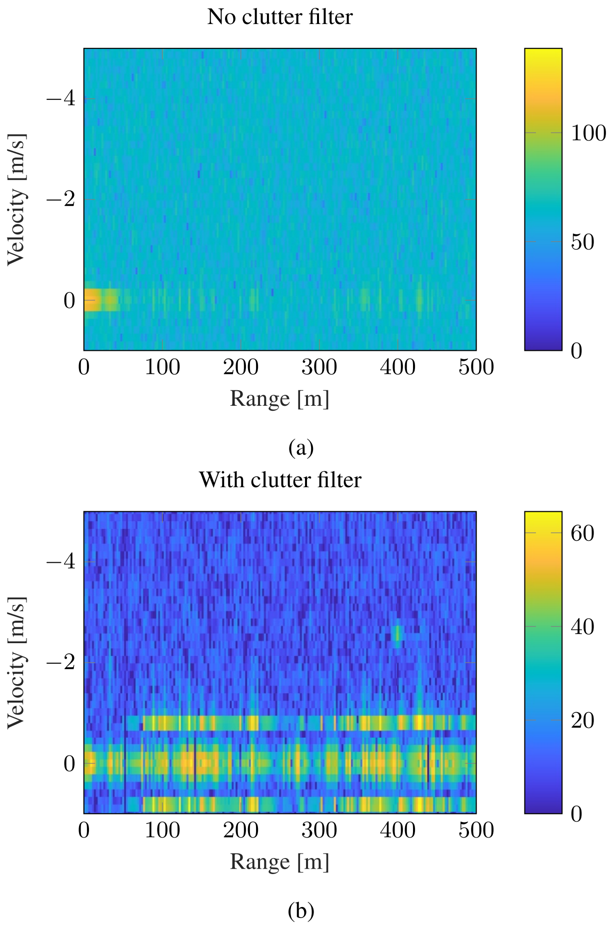


**FIGURE 2** Range-Doppler processed model data. The model emulates the experiment with a non-repeating waveform for the purpose of validating the clutter suppression algorithm. (a) No clutter filtering. The target is obscured by the correlation noise floor due to a strong direct signal with a power 120 dB stronger than the thermal noise at 0 dB. Some clutter with randomised power on [30, 80] dB is weakly visible, centred at zero Doppler. (b) Clutter suppression by applying the Sequential CLEAN algorithm. Here, the correlation noise floor is suppressed and the target with a power 45 dB above the noise floor is clearly visible at a distance of 400 m and velocity of −2.5 m/s. The clutter filtering produces a residual edge effect in the ±0.9 m/s Doppler channel.

## 3.1 | Transmitter

To generate the signal, the transmitter utilises the ADS7-V2 [51] evaluation board in combination with the AD9162-FMC-EBZ [52] digital to analog (DAC) converter. The board has an accessible memory of approximately 4 GB in which predefined waveforms can be downloaded. This makes it possible to design waveforms using, for example, MATLAB [53]. The DAC can sample 16 bits at 12.6 GS/s, thus allowing for direct signal synthesising in the L-Band. It also has built-in digital up-conversion and an interpolation filter with a maximum interpolation order of 24. This permits the transmission of long waveforms since the baseband sampling frequency only needs to satisfy Nyquist's theorem.

In a system consisting of separate transmitter and receiver units, an important aspect is synchronisation in time and frequency. Currently, the system makes use of GNSS units [54] for both synchronisations. There are, however, other ways the system could be synchronised, see ref. [44, 55]. Time synchronisation is maintained by sending a pulse-per-second signal, from the GNSS unit to the ADS7-V2 board, which effectively acts as a trigger. The GNSS unit also has a GNSS disciplined 10 MHz oscillator, which is used as frequency reference to the DAC's internal voltage controlled oscillator.

After the signal has been generated, it is band-pass filtered and amplified by a class A amplifier. The amplifier has a gain of 33 dB and a maximum output power of 2 W. Since the average output power from the DAC is approximately −9 dBm, the output power after amplification is 24 dBm.

The transmitter unit is presented in Figure 4. In addition to the components described above, the transmitter also consist of a mini-PC, that acts as a control unit, lithium-ion polymer batteries that power the electronics, and a 2 × 2 element antenna, with an estimated directivity gain of 10.8 dB. The complete system weighs 4.2 kg and could easily be mounted on an UAV to perform bistatic experiments with a moving transmitter.

The system was characterised in terms of correlation losses (Equation (5)) by connecting the amplifier output directly to the receiver chain, that is, looped connection. The input power to the transmitter amplifier was then increased in steps of 1 dB, starting from −18 dBm and going up to 9 dBm. The input power to the receiver chain was kept constant. As can be seen in Figure 5, the loss is moderate for all input powers and only 0.1 dB for −9 dBm. It should be noted that the output power probably saturates at around 0 dBm, as indicated by the Peak to Average Power Ratio (PAPR) [39]. This measurement setup will also include correlation losses introduced by other components. However, these are negligible compared to those of the amplifier, as the losses for −18 dBm to −11 dBm input power is only 0.03 dB.

The correlation loss does not give detailed information about the correlation sidelobes. As a further verification, the normalised correlation response for three different input powers (−9 dBm, − 1 dBm, and 9 dBm) can be seen in Figure 6. The characteristics are similar for all traces. Zooming in on the peaks, it can be seen that the reduction in peak strength is equivalent to the losses in Figure 5, that is, the strength of the CNF is constant, while the main peak is slightly reduced in strength.

As expected, the PAPR is much more sensitive to input power than the correlation loses. The PAPR of the digital reference is 12.1, which implies deterioration already at the lowest input power of −18 dBm. Amplitude modulation is important for LPI [6] and LPID properties. For example, if the radar were to disguise itself as a telecommunication signal, it would require the system to handle PAPRs of 10 dB or higher [56]. That being said, high PAPR signals significantly reduce the maximum output power. Thus, in terms of detection performance, a low PAPR waveform is ideal [39].

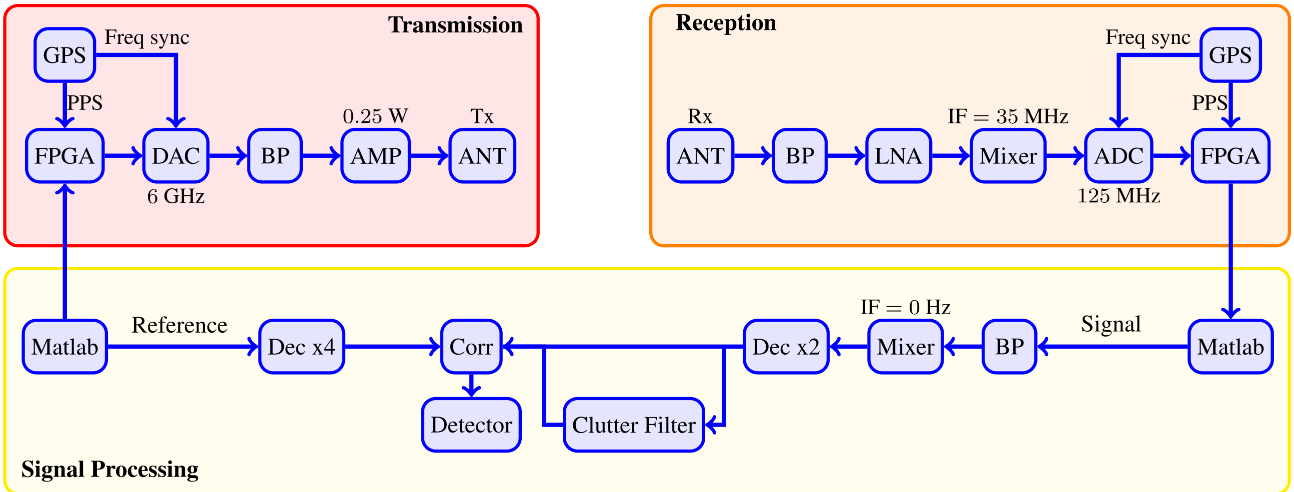


**FIGURE 3** Block diagram of the complete bistatic system. The Signal Processing block is performed offline.

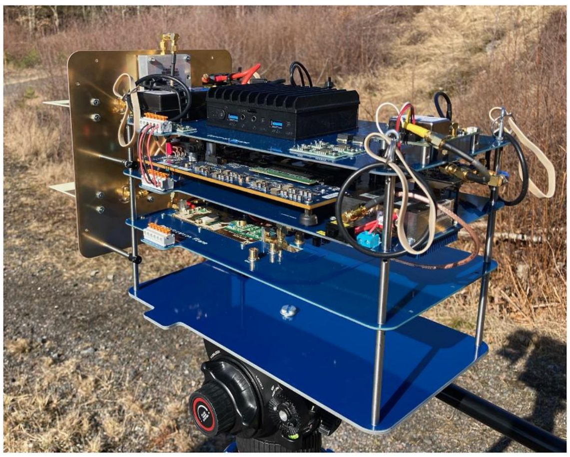

**FIGURE 4** The bistatic radar transmitter used for the experiments. (*Uppermost Plane*) mini-PC, GNSS unit, battery and analog control logic. (*Second Plane*) FPGA, DAC and amplifier. (*Third Plane*) Pulsed 300 W amplifier stage, not used in the experiments. (*Fourth Plane*) For mounting only.

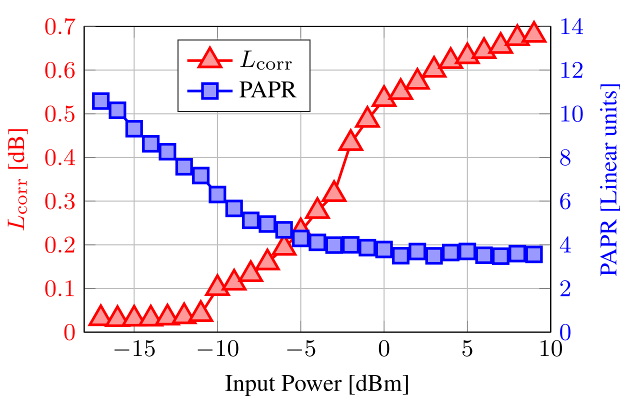


**FIGURE 5** Correlation loss, defined in Equation (5), and Peak to Average Power Ratio (PAPR) as a function of the amplifier's input power.

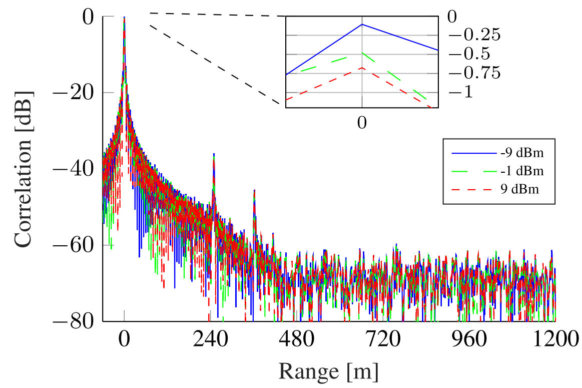


**FIGURE 6** Normalised correlation spectrum, after amplification, for three different input powers. The sidelobe characteristics is effectively independent of input power. The peaks at roughly 250 and 360 m are a result of the rectangular band-pass filter used when generating the waveforms. (Inset) Zoom-in on maximum correlation. A correlation loss of less than 1 dB is measured over the range of input power.

## 3.2 | Receiver

In the receiver, the signal is band-pass filtered, amplified, analog downconverted and sampled by a 14-bit analog to digital converter (ADC). The sampled data is momentarily stored in a field programmable gate array (FPGA) before being sent to a computer. The measurement time is limited by the FPGA's storage capacity, which, at an ADC sampling speed of 125 MS/s, is roughly 0.9 s. Time and frequency synchronisation is performed in the same way as in the transmitter unit.

## 3.3 | Waveforms and sampling frequencies

Two different, continuous wave, pseudo-random noise waveforms have been considered. One waveform repeats every 10 ms, that is, it has a repetition frequency of 100 Hz, whereas the other waveform never repeats. We refer to these waveforms as repeating and non-repeating respectively. The repeating waveform is used as a benchmark because it suffers significantly less from the masking effect problem. Repeating noise could be of interest in applications where LPI properties are of less importance.

Both waveforms are band-pass limited pseudo-random complex Gaussian noise, with a hard rectangular frequency spectrum of 50 MHz, giving a range resolution of 3 m. They were generated by applying a low-pass filter to a sequence of complex pseudo-random noise samples, which were generated by MATLAB's pseudo-random noise generator. The ambiguity function of the signal can be seen in Figure 6.

The ADC sampling rate is restricted to 125 MS/s and, in order to avoid fractional resampling of the reference, the base-band sampling rate of the transmitted signal was set to 250 MS/s, that is, twice that of the ADC. The DAC digitally up-converts the signal to a centre frequency of 1.3 GHz (L-band) and then samples it at a rate of 6 GS/s, using 24-times interpolation. In the receiver, the signal is downconverted to an intermediate centre frequency of 35 MHz before being sampled by the ADC.

### 3.4 | Signal processing

The received signal is further filtered with a digital band-pass filter before being digitally downconverted to baseband and downsampled by a factor of two, resulting in a sampling rate of 62.5 MS/s. Inspired by conventional pulsed Doppler radar, range and Doppler processing is performed sequentially for both the repeating and non-repeating waveforms (also referred to as batch processing) [47, 57]. That is, the received signal is split into batches, where each batch is treated as a pulse. The Doppler shift is then extracted by calculating the inter-pulse phase variation with a Fast Fourier Transform. To reduce Doppler sidelobes, a Hann window is applied [58]. Since the repeating waveform has a batch length (or pulse length) of 10 ms, the non-repeated waveform is also split into batches of 10 ms. This gives a maximum unambiguous velocity of 5.7 m/s. Clutter filtering is performed after decimation, but before the signal is separated into batches.

After the range-Doppler map has been calculated, a threshold detector is applied. The detector uses diagonal cells as reference cells to avoid target sidelobes contaminating the detector. The maximum threshold for which the target clears the detector is used when comparing the different results. The bistatic range is treated in the same way as in a monostatic radar, that is, time of flight divided by two. A full bistatic range treatment would require significantly better angle resolution. Stretch processing is not considered.

## 4 | MEASUREMENT SCENARIO

The bistatic measurement scenario considered is illustrated in Figure 7, with the radar parameters and the measurement ranges presented in Table 1 and Table 2, respectively. This scenario is compared to a monostatic measurement scenario

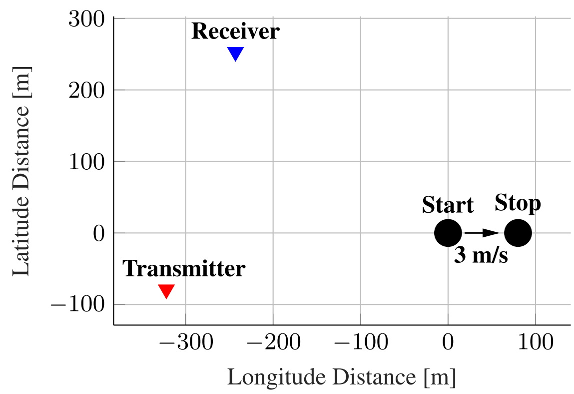


**FIGURE 7** The bistatic measurement scenario of the experiment. Distances and bearings between the four points are detailed in Table 2. The target Unmanned Aerial Vehicle (UAV) is flown at an altitude of 150 m above sea level while the receiver and the transmitter are located at 120 and 100 m above sea level, respectively. In the monostatic scenario, the transmitter is located at the receiver site.

**TABLE 1** Radar parameters

| | | |
|---|---|---|
| Transmitted power | $P_T$ | 0.25 W |
| Transmitter antenna gain | $G_T$ | 10.8 dB |
| Receiver antenna gain | $G_R$ | 10.8 dB |
| Wavelength | $\lambda$ | 0.23 m |
| Integration time | $\tau_I$ | 0.9 s |
| Target RCS | $\sigma$ | 0.01 m$^2$ |
| Reference temperature | $T_0$ | 290 K |
| Noise Figure | $F$ | 3 dB |
| Compound loss[a] | $L$ | 6 dB |

[a]Correlation losses, receiver losses, signal processing losses, Doppler resolution losses, etc.

**TABLE 2** Distances and directions between the points in Figure 7

| | Distance [m] | Compass Bearing [°] |
|---|---|---|
| Tx-start | 332 | 86.2 |
| Tx-stop | 410 | 88.9 |
| Rx-start | 351 | 136.2 |
| Rx-stop | 410 | 128.1 |
| Tx-Rx | 341 | 23.4 |

where the transmitter is instead located at the receiver site, corresponding to $S = 1.5$ m and $\varphi \simeq 0$ in Figure 1. In both scenarios, line of sight to the target is maintained and the signal-to-noise ratio (SNR) is approximately equal. The test was carried out under non-ideal conditions, where the surroundings are full of clutter objects, such as hills, trees, buildings, power lines etc., as seen in Figure A1 of Appendix A. Acting as a target was a DJI Matrice 600 UAV, flying at a constant speed of 3 m/s. The UAV RCS is estimated to 0.01 m$^2$.

Using Equations (1 and 2), the expected SNR and measured velocity can be calculated, see Table 3. According to

Equation (3) the velocity resolution will be 0.264 m/s, compared to 0.128 m/s if stretch processing would have been applied. Essentially, the target signal will spread into two Doppler bins.

## 5 | RESULTS

We start by examining the results for the repeating waveform, as these results serve as a benchmark for the non-repeating waveform. Then, the results for the non-repeating waveform, both with and without clutter filtering, is presented. The results can be seen in Figures 8 and 9. As in Figure 2, the colour scale reference level has been selected such that 0 dB approximates the average thermal noise floor level. However, the thermal noise floor has not been thoroughly measured and the possibility of other noise sources have not been ruled out. The signal strength from the close range clutter interference is 40 dB lower in the bistatic measurements and, consequently, the CNF is reduced by an equal amount, as seen by comparing Figure 9a with Figure 9b.

### 5.1 | Repeating waveform

In the bistatic measurement, the target is clearly visible at a range of 362 m and at a speed of 2.7 m/s. The target signal spreads into two Doppler bins, as expected when no stretch processing is performed. It passes the detector with a maximum threshold of 41 dB. The strong signal present at 170 m is the direct signal interference (340 m/2 = 170 m) from the transmitter. In the monostatic setup, the direct signal interferes at roughly 0 m.

**TABLE 3** Expected signal-to-noise ratio (SNR) and velocity

| | SNR [dB] | Velocity [m/s] |
|---|---|---|
| Monostatic (start) | 43 | −2.1 |
| Monostatic (stop) | 40 | −2.4 |
| Bistatic (start) | 43 | −2.5 |
| Bistatic (stop) | 40 | −2.7 |

Comparing the bistatic results to the monostatic results, it is clearly seen that there is significantly more clutter present in the monostatic case and, as a consequence, we are limited by correlation noise. Still, the target is visible at a range of 389 m and at a speed of 2.3 m/s, and passes the detector with a threshold of 25 dB.

### 5.2 | Non-repeating waveform

First, we will address the obvious problem, which is the significant correlation noise present in the monostatic results. The CNF is approximately 62 dB above the thermal noise floor, or 21 dB above the target signal level. Significant suppression of close range clutter is required to detect the target. However, in the bistatic setup with separated receiver and transmitter, we get 40 dB lower interference from clutter close to the receiver. The target is now detectable at 341 m, with a speed of 2.6 m/s and clears the detector with a threshold of 21 dB.

By applying 100 iterations of the Sequential CLEAN algorithm, the CNF is further suppressed by approximately 23 and 19 dB for the monostatic and bistatic setup respectively. For the monostatic setup, this is insufficient, as the target is still engulfed in correlation noise. In the bistatic setup, the target now passes the detector with a threshold of 40 dB, reaching the same performance as the repeating waveform, competing primarily with thermal noise.

## 6 | DISCUSSION

From the results, we can conclude that spatial separation between the transmitter and receiver is an effective tool to mitigate the detrimental effect of direct signal and strong close

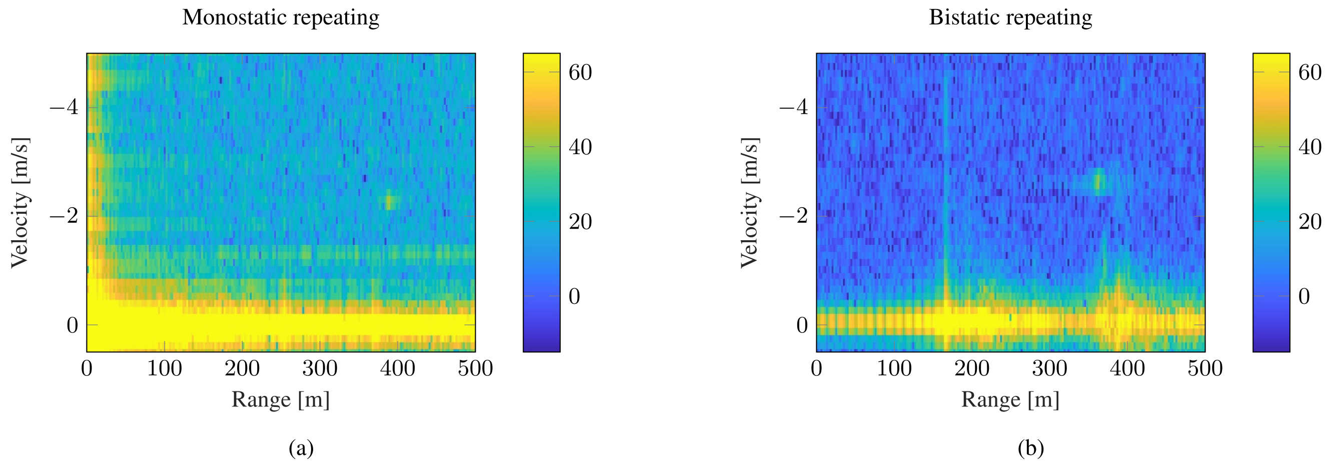


**FIGURE 8** Range-Doppler processed data with repeating waveform and no post-processing. (a) Monostatic setup. The target is visible at ≃ 40 dB, with the correlation noise floor at ≃ 20 dB. (b) Bistatic setup. The target is visible at ≃ 40 dB, with the correlation noise floor at ≃ 0 dB.

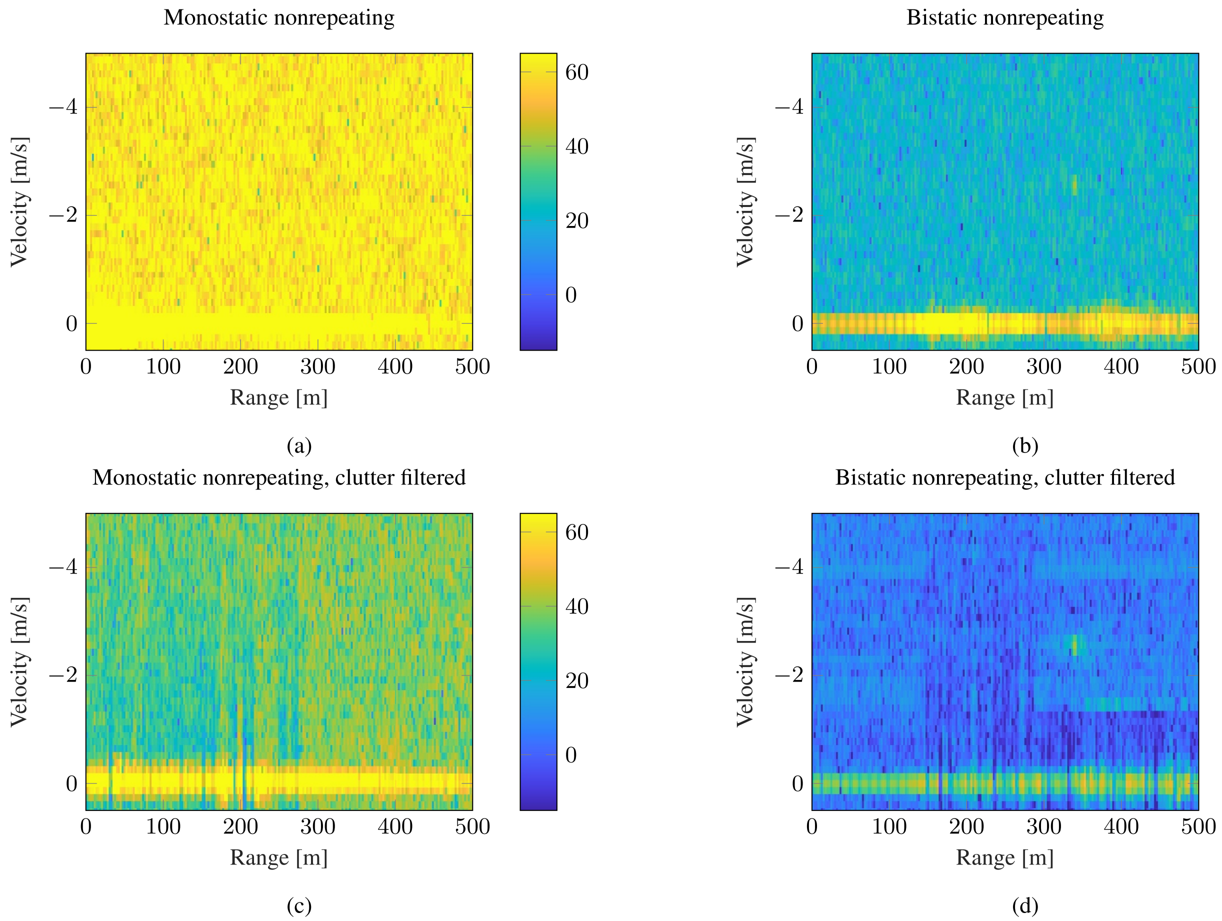


**FIGURE 9** Range-Doppler processed data with non-repeating waveform, with and without post-processing. (a) Monostatic setup where the target is obscured by the correlation noise floor at $\simeq$ 60 dB. (b) Bistatic setup where the target is visible at $\simeq$ 40 dB, with the correlation noise floor at $\simeq$ 20 dB. (c) Monostatic setup with post-process clutter filtering. The correlation noise floor has been reduced to $\simeq$ 40 dB, leaving the target still obscured. (d) Bistatic setup with post-process clutter filtering. The correlation noise floor has been reduced to $\simeq$ 0 dB, with the target visible at $\simeq$ 40 dB.

range clutter interference. It should be noted that careful design of the architecture for a monostatic system could reduce the antenna crosstalk. However, for a ground based continuous wave system there will, realistically, always be close range clutter interference, which is not the case for a bistatic setup. Actually, the main interference in the monostatic setup is due to ground clutter a few metres in front of the antennas. Bistatic operation reduces the close range clutter interference, without requiring changes in the system architecture.

We observe that the clutter suppression performs worse in experiment than in the model. The reason for this is assumed to be because of model mismatch with dense clutter and complicated multipath channels. Furthermore, the model does not include unintended phase fluctuations. We have also tested conventional CLEAN [50] as well as the lattice filter approach [21, 22] and found them both insufficient for the challenging clutter environment here, while the Sequential CLEAN algorithm performs significantly better. To further improve the clutter suppression, we expect a simultaneous estimate and subtraction of a section of the clutter environment might do better, for example, with the least mean square algorithms of refs. [27, 59]. Additionally, estimating clutter positions off-the-grid by resampling could improve the CLEAN algorithm performance at the cost of increased computational complexity.

With a multi-channel receiver, adaptive beamforming [47, 60, 61] could further suppress the direct signal and other strong scatterers. How many scatterers that can be suppressed depends on the number of available channels.

Using GNSS to synchronise the frequency does not introduce any obvious issues. The time synchronisation is not thoroughly investigated. However, from the many measurements performed, it was seen that the position of the direct signal differed about $\pm 6$ m, which is consistent with the specifications of the GNSS unit [54]. For most applications this precision is adequate. However, if a military system is considered, it is undesirable to rely solely on GNSS. Implementation of other synchronisation solutions has to be investigated.

## 7 | CONCLUSION

In summary, the system we have developed and analysed is capable of both monostatic and bistatic noise radar operation. We have showed the benefits of separation of transmitter and receiver in the reduction of interference due to close range clutter. Additionally, we have implemented off-line processing to further suppress clutter. These results serve to illustrate some of the challenges in monostatic noise radar, and how they can be solved by bistatic separation. We expect that significant further suppression can be achieved by adaptive beamforming with a multichannel receiver.

## AUTHOR CONTRIBUTION

**Martin Ankel**: Conceptualisation; Data curation; Formal analysis; Investigation; Methodology; Software; Validation; Visualisation; Writing – original draft; Writing - Review & Editing. **Robert Jonsson**: Conceptualisation; Data curation; Formal analysis; Investigation; Methodology; Software; Validation; Visualisation; Writing – original draft; Writing - Review & Editing. **Tomas Bryllert**: Conceptualisation; Data curation; Investigation; Supervision; Validation; Writing – original draft; Writing - Review & Editing. **Lars Ulander**: Conceptualisation; Project administration; Supervision; Writing – original draft; Writing - Review & Editing. **Per Delsing**: Conceptualisation; Project administration; Resources; Supervision; Writing – original draft; Writing - Review & Editing; Funding acquisition.

## ACKNOWLEDGEMENTS

The authors thank P. Johanisson for assisting with the measurements and K. Falk for helpful discussions. The authors acknowledge the Knut and Alice Wallenberg (KAW) foundation for funding through the Wallenberg Centre for Quantum Technology and internal support from Saab. Knut and Alice Wallenberg foundation, Grant/Award Number: KAW 1017.0449.

## CONFLICT OF INTEREST

We have no conflicts of interest to disclose.

## DATA AVAILABILITY STATEMENT

The data that support the findings of this study are available from the corresponding author upon reasonable request.

## ORCID

*Martin Ankel* https://orcid.org/0000-0003-2259-4500

## REFERENCES

1. Dawood, M., Narayanan, R.M.: Generalised wideband ambiguity function of a coherent ultrawideband random noise radar. IEE Proc. - Radar, Sonar Navig. 150(5), 379–386 (2003). https://doi.org/10.1049/ip-rsn:20030702
2. Axelsson, S.R.J.: Noise radar using random phase and frequency modulation. IEEE Trans. Geosci. Rem. Sens. 42(11), 2370–2384 (2004). https://doi.org/10.1109/tgrs.2004.834589
3. Axelsson, S.R.J.: Generalized ambiguity functions for ultra wide band random waveforms. In: 2006 International Radar Symposium, pp. 1–4. IEEE, Kraków, Poland (2006)
4. Liu, G.S., et al.: Random signal radar - a winner in both the military and civilian operating environments. IEEE Trans. Aero. Electron. Syst. 39(2), 489–498 (2003). https://doi.org/10.1109/taes.2003.1207261
5. Thayaparan, T., Daković, M., Stanković, L.: Mutual interference and low probability of interception capabilities of noise radar. IET Radar, Sonar Navig. 2(4), 294–305 (2008). https://doi.org/10.1049/iet-rsn:20070146
6. Galati, G., et al.: Counter-interception and counter-exploitation features of noise radar technology. Rem. Sens. 13(22), 1–22 (2021). https://doi.org/10.3390/rs13224509
7. Thayaparan, T., Wernik, C. 'Noise Radar Technology Basics', Ottawa: Defence R&D Canada, (2006). Tech. Report
8. Horton, B.M.: Noise-modulated distance measuring systems. Proc. IRE 47(5), 821–828 (1959). https://doi.org/10.1109/jrproc.1959.287275
9. Narayanan, R.M., Dawood, M.: Doppler estimation using a coherent ultrawide-band random noise radar. IEEE Trans. Antenn. Propag. 48(6), 868–878 (2000). https://doi.org/10.1109/8.865218
10. Lukin, K.A., et al.: Ka-band bistatic ground-based noise waveform SAR for short-range applications. IET Radar, Sonar Navig. 2(4), 233–243 (2008). https://doi.org/10.1049/iet-rsn:20080017
11. Malanowski, M., Kulpa, K.S.: Detection of moving targets with continuous-wave noise radar: theory and measurements. IEEE Trans. Geosci. Rem. Sens. 50(9), 3502–3509 (2012). https://doi.org/10.1109/tgrs.2011.2181521
12. Susek, W., Stec, B.: Stec, B.: 'Through-the-wall detection of human activities using a noise radar with microwave quadrature correlator'. IEEE Trans. Aero. Electron. Syst. 51(1), 759–764 (2015). https://doi.org/10.1109/taes.2014.130003
13. Susek, W., Kniola, M., Stec, B.: Buried objects detection using noise radar. In: 2018 22nd International Microwave and Radar Conference (MIKON), pp. 461–463. IEEE, Poznań, Poland (2018)
14. Wasserzier, C., Stove, A.G., Lukin, K.A.: Verification of a continuous wave noise radar. In: 20th International Radar Symposium (IRS 2019), pp. 1–10. IEEE, Ulm, Germany (2019)
15. Savci, K., et al.: Trials of a noise-modulated radar demonstrator – first results in a marine environment. In: 20th International Radar Symposium (IRS 2019), pp. 1–9. IEEE, Ulm, Germany (2019)
16. Wasserzier, C., Galati, G.: First experimental results on the feasibility of noise radar systems on fast moving platforms. Electron. Lett. 55(6), 344–345 (2019). https://doi.org/10.1049/el.2018.7511
17. Galati, G., et al.: Noise radar technology: waveforms design and field trials. Sensors 21(9), 3216 (2021). https://doi.org/10.3390/s21093216
18. Kulpa, K.S., Czekala, Z.: Masking effect and its removal in PCL radar. IEE Proc. - Radar, Sonar Navig. 152(3), 174–178 (2005). https://doi.org/10.1049/ip-rsn:20045026
19. Axelsson, S.R.J.: Analysis of random step frequency radar and comparison with experiments. IEEE Trans. Geosci. Rem. Sens. 45(4), 890–904 (2007). https://doi.org/10.1109/tgrs.2006.888865
20. Stec, B., Susek, W.: Theory and measurement of signal-to-noise ratio in continuous-wave noise radar. Sensors 18(5), 1445 (2018). https://doi.org/10.3390/s18051445
21. Kulpa, K.S.: Simple Sea clutter canceller for noise radar. In: 2006 International Radar Symposium, pp. 1–4. IEEE, Kraków, Poland (2006)
22. Kulpa, K.S.: Signal Processing in Noise Waveform Radar. Artech House (2013)
23. Axelsson, S.R.J.: Suppression of noise floor and dominant reflectors in random noise radar. In: 2006 International Radar Symposium, pp. 1–4. IEEE, Kraków, Poland (2006)
24. Colone, F., Cardinali, R., Lombardo, P.: Cancellation of clutter and multipath in passive radar using a sequential approach. In: 2006 IEEE Conference on Radar, pp. 1–7. IEEE, Verona, NY (2006)
25. Axelsson, S.R.J.: Random noise radar/sodar with ultrawideband waveforms. IEEE Trans. Geosci. Rem. Sens. 45(5), 1099–1114 (2007). https://doi.org/10.1109/tgrs.2007.893742
26. Meller, M.: Cheap cancellation of strong echoes for digital passive and noise radars. IEEE Trans. Signal Process. 60(5), 2654–2659 (2012). https://doi.org/10.1109/tsp.2012.2187286
27. Meller, M., Tujaka, S.: Processing of noise radar waveforms using block least mean squares algorithm. IEEE Trans. Aero. Electron. Syst. 48(1), 749–761 (2012). https://doi.org/10.1109/taes.2012.6129668

28. Ansari, F., Taban, M.R.: Implementation of sequential algorithm in batch processing for clutter and direct signal cancellation in passive bistatic radars. In: 2013 21st Iranian Conference on Electrical Engineering (ICEE), pp. 1–6. IEEE, Mashhad, Iran (2013)
29. Fry, R.D., Gray, D.A.: CLEAN deconvolution for sidelobe suppression in random noise radar. In: 2008 International Conference on Radar, pp. 209–212. IEEE, Adelaide (2008)
30. Bai, X., et al.: Clutter cancellation in passive radar using batch-based CLEAN technique. EURASIP J. Appl. Signal Process. 63(2021), 1–19 (2021). https://doi.org/10.1186/s13634-021-00769-9
31. Kulpa, J.S.: Noise radar sidelobe suppression algorithm using mismatched filter approach. Int. J. Microw. Wirel. Technol. 8(6), 865–869 (2016). https://doi.org/10.1017/s1759078716000945
32. Nelander, A.: Inverse filtering for noise radar processing. In: 2006 International Radar Symposium, pp. 1–4. IEEE, Kraków, Poland (2006)
33. Shareef, E., Dawood, M., Boehm, J.: Experimental results to reduce sidelobes in random noise and linear frequency modulated signals. Electron. Lett. 53(8), 564–566 (2017). https://doi.org/10.1049/el.2017.0466
34. Raout, J., Santori, A., Moreau, E.: Passive bistatic noise radar using DVB-T signals. IET Radar, Sonar Navig. 4(3), 403–411 (2010). https://doi.org/10.1049/iet-rsn.2009.0053
35. Xu, X., Narayanan, R.M.: Range sidelobe suppression technique for coherent ultra wide-band random noise radar imaging. IEEE Trans. Antenn. Propag. 49(12), 1836–1842 (2001). https://doi.org/10.1109/8.982467
36. Haghshenas, H., Nayebi, M.M.: Suppressing sidelobe levels in random phase modulated radar. In: 2011 IEEE RadarCon (RADAR), pp. 530–532. IEEE, Kansas City (2011)
37. Kulpa, J.S., Maślikowski, L.u., Malanowski, M.: Filter-based design of noise radar waveform with reduced sidelobes. IEEE Trans. Aero. Electron. Syst. 53(2), 816–825 (2017). https://doi.org/10.1109/taes.2017.2665145
38. De.Palo, F., Galati, G.: Range sidelobes attenuation of pseudorandom waveforms for civil radars. In: 2017 European Radar Conference (EURAD), pp. 114–117. IEEE, Nuremberg (2017)
39. Palo, F.D., et al.: Introduction to noise radar and its waveforms. Sensors 20(18), 5187 (2020). https://doi.org/10.3390/s20185187
40. Savci, K., Galati, G., Pavan, G.: Low-PAPR waveforms with shaped spectrum for enhanced low probability of intercept noise radars. Rem. Sens. 13(12), 2372 (2021). https://doi.org/10.3390/rs13122372
41. Purdy, D.S.: Receiver antenna scan rate requirements needed to implement pulse chasing in a bistatic radar receiver. IEEE Trans. Aero. Electron. Syst. 37(1), 285–288 (2001). https://doi.org/10.1109/7.913687
42. Willis, N.J.: Bistatic Radar, 2nd ed. SciTech Publishing (2005)
43. Willis, N.J., Griffiths, H.D. (eds.) Advances in Bistatic Radar. SciTech Publishing, Inc. (2007)
44. Malanowski, M., Roszkowski, P.: Bistatic noise radar using locally generated reference signal. In: 2011 12th International Radar Symposium (IRS), pp. 544–549. IEEE, Leipzig (2011)
45. Roszkowski, P., Malanowski, M.: Bistatic noise radar demonstrator with phase-interferometry for bearing determination. In: 2014 IEEE Radar Conference, pp. 0962–0967. IEEE, Cincinnati (2014)
46. Kulpa, K.S.: The effect of target presence in reference channel of bistatic noise radar. In: 2008 International Radar Symposium, pp. 1–4. IEEE, Wroclaw, Poland (2008)
47. Axelsson, S.R.J.: Noise radar for range/Doppler processing and digital beamforming using low-bit ADC. IEEE Trans. Geosci. Rem. Sens. 41(12), 2703–2720 (2003). https://doi.org/10.1109/tgrs.2003.816665
48. Kulpa, K.S., Misiurewicz, J.: Stretch processing for long integration time passive covert radar. In: 2006 CIE International Conference on Radar, pp. 1–4. IEEE, Shanghai (2006)
49. Wasserzier, C.: Exploiting the low Doppler tolerance of noise radar to perform precise velocity measurements on a short set of data. Signals 2(1), 25–40 (2021). https://doi.org/10.3390/signals2010003
50. Högbom, J.A.: Aperture synthesis with a non-regular distribution of interferometer baselines. Astron. Astrophys. Suppl. 15, 417–426 (1974)
51. 'ADS7-V2EBZ High Speed Evaluation BOARD'. Analog Devices, User Guide. [Online]. https://wiki.analog.com/resources/eval/ads7-v2 (2021). Accessed 18 Jan 2022
52. AD9161/AD9162/AD9163/AD9164 User Guide'. Analog Devices, User Guide UG-1526, rev 0. [Online]. https://www.analog.com/media/en/technical-documentation/user-guides/AD9%20161-9162-9163-9164-UG-1526.pdf (2019). Accessed 18 Jan 2022
53. 'MATLAB'. The MathWorks Inc. Software, version, R2020b. [Online]. https://se.mathworks.com. Accessed 10 Feb 2021
54. 'iSync+ Smart GXClok-500 Manual'. Spectratime, Manual, rev 2.10. [Online]. https://www.orolia.com/product/gxclok-500-gps-gnss-ocxo-clock-module/ (2017). Accessed 18 Jan 2022
55. Weiß, M.: Synchronisation of bistatic radar systems. In: IGARSS 2004. 2004 IEEE International Geoscience and Remote Sensing Symposium, vol. 3, pp. 1750–1753. Anchorage (2004)
56. Dahlman, E., Parkvall, S., Sköld, J.: '5G NR: The Next Generation Wireless Access Technology', 1st ed. Academic Press, Inc., USA (2018)
57. Axelsson, S.R.J.: On the theory of noise Doppler radar. In: IGARSS 2000. IEEE 2000 International Geoscience and Remote Sensing Symposium. Taking the Pulse of the Planet: The Role of Remote Sensing in Managing the Environment. Proceedings (Cat. No.00CH37120), vol. 2, pp. 856–860. IEEE, Honolulu (2000)
58. Harris, F.J.: On the use of windows for harmonic analysis with the discrete Fourier transform. Proc. IEEE 66(1), 51–83 (1978). https://doi.org/10.1109/proc.1978.10837
59. Meller, M., Tujaka, S.: Block least mean squares processing of noise radar waveforms. In: 2009 IEEE Radar Conference, pp. 1–6. IEEE, Pasadena (2009)
60. Van Veen, B.D., Buckley, K.M.: Beamforming: a versatile approach to spatial filtering. IEEE ASSP Mag. 5(2), 4–24 (1988). https://doi.org/10.1109/53.665
61. Nickel, U.: Principles of adaptive array processing. In: Advanced Radar Signal and Data Processing, pp. 5.1–5.20. RTO, Neuilly-sur-Seine, France (2006). Educational Notes RTO-EN-SET-086, Paper 5


**How to cite this article:** Ankel, M., et al.: Bistatic noise radar: demonstration of correlation noise suppression. IET Radar Sonar Navig. 17(3), 351–361 (2023). https://doi.org/10.1049/rsn2.12345

# APPENDIX A

## A | Transmitter location

**FIGURE A1** Location of the transmitter in the bistatic setting. The illuminated environment consists of several clutter objects, such as: trees, power lines, hills, radio towers, etc., which makes it a realistic setting for ground based radar systems